Cancer therapy improvement with mesoporous silica nanoparticles combining photodynamic and photothermal therapy

2014 Nanotechnology 25 285701

(http://iopscience.iop.org/0957-4484/25/28/285701)

IOP Publishing Nanotechnology
Nanotechnology **25** (2014) 285701 (9pp) doi:10.1088/0957-4484/25/28/285701

Cancer therapy improvement with mesoporous silica nanoparticles combining photodynamic and photothermal therapy

Z X Zhao[1,4], Y Z Huang[1,4], S G Shi[1], S H Tang[1], D H Li[3] and X L Chen[1,2]

[1] Department of Chemistry, College of Chemistry and Chemical Engineering, Xiamen University, Xiamen 361005, People's Republic of China
[2] State Key Laboratory of Chemo/Biosensing and Chemometrics, Hunan University, Changsha 410082, People's Republic of China
[3] Cancer Research Center, College of Medicine, Xiamen University, Xiamen 361005, People's Republic of China

E-mail: chenxl@xmu.edu.cn

Received 13 March 2014, revised 15 May 2014
Accepted for publication 5 June 2014
Published 27 June 2014

Abstract

In this work, we develop novel mesoporous silica composite nanoparticles (*hm*-SiO_2(AlC_4Pc)@Pd) for the co-delivery of photosensitizer (PS) tetra-substituted carboxyl aluminum phthalocyanine (AlC_4Pc) and small Pd nanosheets as a potential dual carrier system to combine photodynamic therapy (PDT) with photothermal therapy (PTT). In the nanocomposite, PS AlC_4Pc was covalently conjugated to a mesoporous silica network, and small Pd nanosheets were coated onto the surface of mesoporous silica by both coordination and electrostatic interaction. Since small Pd nanosheets and AlC_4Pc display matched maximum absorptions in the 600–800 nm near-infrared (NIR) region, the fabricated *hm*-SiO_2(AlC_4Pc)@Pd nanocomposites can generate both singlet oxygen and heat upon 660 nm single continuous wavelength (CW) laser irradiation. *In vitro* results indicated that the cell-killing efficacy by simultaneous PDT/PTT treatment using *hm*-SiO_2(AlC_4Pc)@Pd was higher than PDT or PTT treatment alone after exposure to a 660 nm CW-NIR laser.

S Online supplementary data available from stacks.iop.org/NANO/25/285701/mmedia

Keywords: hollow mesoporous silica nanoparticles, tetra-substituted carboxyl aluminum phthalocyanine (AlC_4Pc) photosensitizer, Pd nanosheets, combinational therapy

(Some figures may appear in colour only in the online journal)

1. Introduction

Photodynamic therapy (PDT) has emerged as a new kind of cancer treatment modality during the past two decades. PDT is based on the concept that a photosensitizer (PS) can preferably accumulate in the cancer and generate reactive oxygen species (ROS) upon proper light irradiation to destroy the lesion [1, 2]. To date, several classes of PSs, including porphyrins, chlorines, metal phthalocyanines (MPcs), phenothiazinium compounds, etc, have been officially approved or are under preclinical testing for PDT [3, 4]. However, most PSs are hydrophobic species and are prone to aggregate after intravenous injection, which will decrease the efficacy of PDT [5]. To improve the water solubility of PSs, as well as to enhance their delivery into cancer cells, various carriers have been developed for the effective delivery of PSs [5–16]. These colloidal carriers can protect PSs from aggregation in a physiological environment and ensure their homogeneous distribution in target tissues. Among them, mesoporous silica nanoparticles (MSNs) have gained popular use as PS carriers owing to their high pore volume, large surface area, good biocompatibility and easy surface functionalization [9–16].

[4] These authors contributed equally to this work.

In order to further improve the therapeutic index of PDT, a new strategy in current nanotechnology is to combine PDT with other treatment modalities, e.g. photothermal therapy (PTT) [15–21]. By loading PSs onto near-infrared (NIR) absorption photothermal nanomaterials, such as Au, carbon and Pd nanostructures, researchers have investigated the combined therapeutic effect of PDT and PTT [15, 17–21]. These nanocomposites showed a synergistic effect of combining PDT and PTT both *in vitro* and *in vivo* under NIR irradiation.

Although high therapeutic outcomes can be obtained via synergistic effects in most of the studies mentioned above, two different wavelength lasers were usually required to excite PDT and PTT separately due to the absorption mismatch of photothermal reagents and PSs at NIR region. Using two lasers for sequential irradiation of the composite nanostructure will complicate the treatment process, as it is difficult to focus two laser beams on the same position. Thus, developing a simple and effective strategy for simultaneous PDT and PTT treatment is highly desirable.

In this work, we describe a novel type of nanocomposite based on small Pd nanosheets covered with hollow mesoporous nanoparticles functionalized with a PS drug, tetra-substituted carboxyl aluminum phthalocyanine (AlC_4Pc). In the nanocomposite, AlC_4Pc, a potential second-generation PS displaying strong absorption in the 600–800 nm phototherapeutic window and high efficiency in the photogeneration of singlet-oxygen [13] were covalently conjugated to the mesoporous silica network, and small Pd nanosheets, which also exhibited high absorption in the 600–800 nm NIR region and high photothermal conversion efficiency [22], were modified on the surface of mesoporous silica by both electrostatic and coordination interaction. The prepared nanocomposites have the following merits: (i) using the biocompatibility of hollow mesoporous silica nanoparticles as a carrier not only improves the water-solubility of PS molecules, making them more efficient in the photogeneration of singlet oxygen, but also provides a convenient surface for various functionalization; (ii) covalent coupling of PS molecules in the rigid mesoporous structure helps to obviate the degradation of PS in harsh biological environments, and overcomes their premature release; (iii) Pd nanosheets are a new kind of promising photothermal agent due to their strong absorption in the NIR region, high photothermal conversion efficiency, excellent photothermal stability and biocompatibility [22–24]. By changing the synthesis condition, a series of Pd nanosheets with different sizes can be obtained; (IV) more importantly, due to the matched maximum absorptions between small Pd nanosheets and AlC_4Pc in the NIR region, the prepared dual-loaded nanocomposite synchronously exhibited photothermal and photodynamic effects upon single continuous wavelength laser irradiation, which will greatly simplify the experimental process and enhance therapeutic efficiency. We investigate the combination treatment effect of PDT and PTT with the nanocomposite on HeLa cells *in vitro*, and we believe that the results presented here will stimulate advances in the use of silica-based multifunctional nanomaterials for therapeutic applications.

2. Experimental section

2.1. Materials

Pd(II) acetylacetonate ($Pd(acac)_2$), tetraethoxysilane (TEOS), 3-aminopropyltriethoxysilane (APTES) and 3-(4,5-dimethylthiazol-2-yl)-2,5-diphenyltetrazolium bromide (MTT) were purchased from Alfa Aesar. Tetrabutylammonium bromide (TBAB), poly(vinylpyrrolidone) (PVP, MW = 30 000 daltons) and cetyltrimethylammonium bromide (CTAB) were obtained from Sinopharm Chemical Reagent Co. Ltd (Shanghai, China). Tetra-substituted carboxyl aluminum phthalocyanine (AlC_4Pc) was synthesized and purified according to a method in the literature [25]. HeLa cells were purchased from the cell storeroom of the Chinese Academy of Science. All other chemicals were of analytical-reagent grade and were used without further purification. The water used in all experiments was ultra-pure.

2.2. Preparation of hm-SiO_2(AlC_4Pc) nanoparticles

2.2.1. Synthesis of solid SiO_2 nanoparticles ($sSiO_2$). Solid SiO_2 nanoparticles ($sSiO_2$) were obtained using a modified Stöber method. Briefly, 60 ml of ethanol, 1 ml of ultra-pure water and 3 ml of ammonium aqueous solution (~28%) were mixed and stirred for 1 h, then 2.3 ml of TEOS was added. The mixture was stirred for 6 h to get the $sSiO_2$ nanoparticles solution.

2.2.2. Synthesis of the AlC_4Pc silanization precursor (AlC_4Pc-APTES) for grafting onto the mesoporous silica shell. To covalently bind the PS of AlC_4Pc to the mesoporous silica shell, AlC_4Pc was first reacted with APTES in the presence of EDC to form the AlC_4Pc silanization precursor. In a typical procedure, 1 ml (5.0 mg ml^{-1} in DMSO) of AlC_4Pc and 100 μl of APTES were mixed. Next, 10 mg of EDC and 10 mg of NHS were added into the mixture and stirred for 12 h at room temperature.

2.2.3. Synthesis of the AlC_4Pc-covalently-grafted $sSiO_2$@CTAB/SiO_2 ($sSiO_2$@CTAB/SiO_2(AlC_4Pc)). 6 ml of the above prepared $sSiO_2$ nanoparticles solution, 4.0 ml of ethanol and 20 ml water were mixed first. To this solution, 7.5 ml of CTAB solution (75 mg CTAB dissolved in 7.5 ml mixture solution of water and ethanol (v:v = 2:1)) was added and stirred for half an hour. Then 50 μl ammonium aqueous, 125 μl TEOS and various volumes of AlC_4Pc–APTES (e.g. 0, 50, 100, 150, 200 and 250 μl) were added and stirred for 12 h. The AlC_4Pc modified $sSiO_2$@CTAB/SiO_2 nanoparticles were collected by centrifugation, and the amount of unconjugated AlC_4Pc in the supernatant was quantified by the calibration curve of AlC_4Pc at 687 nm (figure S1). The difference between the amount of AlC_4Pc-APTES added for the sol-gel reaction and the amount of AlC_4Pc in the supernatant was used for the determination of the loading amount of AlC_4Pc into the following prepared *hm*-SiO_2(AlC_4Pc) nanoparticles (figure S2).

2.2.4. Preparation of AlC_4Pc modified hollow mesoporous SiO_2 nanoparticles (hm-SiO_2(AlC_4Pc)). To transform $sSiO_2$@CTAB/SiO_2(AlC_4Pc) to *hm*-SiO_2(AlC_4Pc), 10 ml of the above solution containing 50 mg of $sSiO_2$@CTAB/

$SiO_2(AlC_4Pc)$ was added with 232 mg of Na_2CO_3 and the mixture was stirred at 50 °C for 11 h. The prepared products were collected by centrifugation. To remove the surfactant template, the products were re-dispersed in 50 ml ethanol containing 0.6 g NH_4NO_3. The mixture was heated to 45 °C under stirring for 6 h, and then the products were collected by centrifugation and washed with ethanol several times. The procedures were repeated three times.

2.3. Synthesis of hm-$SiO_2(AlC_4Pc)$-NH_2

50 mg of *hm*-$SiO_2(AlC_4Pc)$ was dispersed in 25 ml of ethanol, then 25 μl of water and 25 μl of APTES were added, and the mixture was heated to 45 °C for 8 h. The nanoparticles were washed three times with ethanol, and finally re-dispersed in ethanol for subsequent use.

2.4. Synthesis of hexagonal small Pd nanosheets

10 mg of $Pd(acac)_2$, 32 mg of PVP and 30.6 mg of NaBr were dissolved in 2 ml of N,N-Dimethylpropionamide, and then 4 ml of water was added to the mixture. The resulting homogeneous yellow solution was transferred to a glass pressure vessel. The vessel was then charged with CO to 1 bar and heated at 100 °C for 1.5 h. The obtained dark blue solution was stored at 4 °C for further use.

2.5. Synthesis of hm-$SiO_2(AlC_4Pc)$@Pd

2.0 mg of *hm*-$SiO_2(AlC_4Pc)$-NH_2 were dispersed in 1.0 ml of ultra-pure water, and 125, 250 and 500 μg of Pd nanosheets were added. After stirring for 30 min, the resultant products were collected by centrifugation, washed with water and re-dispersed in PBS solution.

According to the calibration curve of Pd nanosheets (figure S3), the loading amount of Pd nanosheets on the *hm*-$SiO_2(AlC_4Pc)$-NH_2 can be determined by the difference between the added Pd amounts and the Pd in the supernatant after centrifuging the *hm*-$SiO_2(AlC_4Pc)$@Pd.

2.6. Singlet oxygen detection

To assess the generation of singlet oxygen ($^1O_2$) from *hm*-$SiO_2(AlC_4Pc)$@Pd, 1,3-diphenylisobenzofuran (DPBF) was used as a probe molecule. DPBF can react irreversibly with $^1O_2$ to cause a decrease in the DPBF absorption at about 400 nm. In a typical process, 50 μl of DPBF (1.5 mg ml^{-1} in acetonitrile) was added into 2 ml of nanoparticles solution (0.2 mg ml^{-1} in acetonitrile), while the controls used DPBF with *hm*-$SiO_2(AlC_4Pc)$ or DPBF with Pd nanosheets in acetonitrile. The solutions were then irradiated with a 660 nm laser source (0.5 W cm^{-2}) for different time periods, and their optical densities at 411 nm were recorded in a UV-2550 spectrophotometer.

2.7. Cellular experiments

2.7.1. Cell culture. HeLa cells were grown in RPMI-1640 culture medium supplemented with 10% calf serum, 1% penicillin and 1% streptomycin in 37 °C under 5% CO_2.

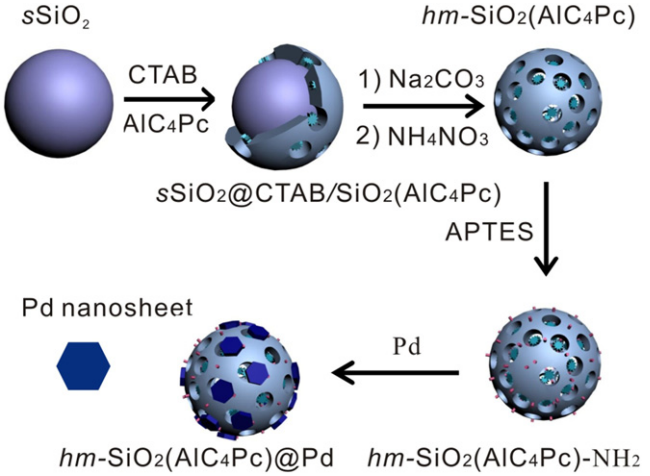

Figure 1. A schematic representation for the preparation of *hm*-$SiO_2(AlC_4Pc)$@Pd nanoparticles.

2.7.2. Cell uptake studies. HeLa cells were seeded in 35 mm culture dishes at a density of about 1×10^5 cells per dish and cultured for 24 h. The cell medium was replaced by fresh medium containing 200 μg ml^{-1} *hm*-$SiO_2(AlC_4Pc)$@Pd and incubated for 4, 8 and 12 h, respectively. After washing the cells with PBS for several times, the cell nucleic were stained with 4′,6′-diamidino-2-phenylindole (DAPI) solution (5 μg mL^{-1}), fluorescence imaging was performed on an Olympus Fluoview 1000 laser-scanning microscope.

2.7.3. Cytotoxicity of the hm-$SiO_2(AlC_4Pc)$@Pd. The cell toxicity of the *hm*-$SiO_2(AlC_4Pc)$@Pd was evaluated by measuring the viability of HeLa cells in the presence of different concentrations of nanoparticles. HeLa cells were seeded in 96-well plates at a density of 10 000 cells per well for 24 h and then added with different amounts of the prepared nanoparticles. After 12, 24 and 48 h of incubation at 37 °C, the viability of the cells was determined by using the MTT assay.

2.7.4. Cancer cell killing efficiency of nanoparticles. To investigate the cancer cell killing efficiency, HeLa cells were incubated with *hm*-$SiO_2(AlC_4Pc)$, *hm*-SiO_2@Pd and *hm*-$SiO_2(AlC_4Pc)$@Pd at the same concentration (100 or 200 μg ml^{-1}) under 37 °C for 12 h, and then exposed to the 660 nm continuous wavelength laser at a power density of 0.5 W cm^{-2} for 7 or 10 min. A standard MTT assay using 3-(4,5-dimethylthiazol-2-yl)-2,5-diphenyltetrazolium bromide (MTT) was conducted to determine cell viability.

In addition, microscopic images of trypan-blue-stained dead cells after incubation with 200 μg ml^{-1} of *hm*-$SiO_2(AlC_4Pc)$@Pd, *hm*-$SiO_2(AlC_4Pc)$ and *hm*-SiO_2@Pd under the irradiation of 660 nm laser (0.5 W cm^{-2}) for 10 min were also observed using the fluorescence microscopy.

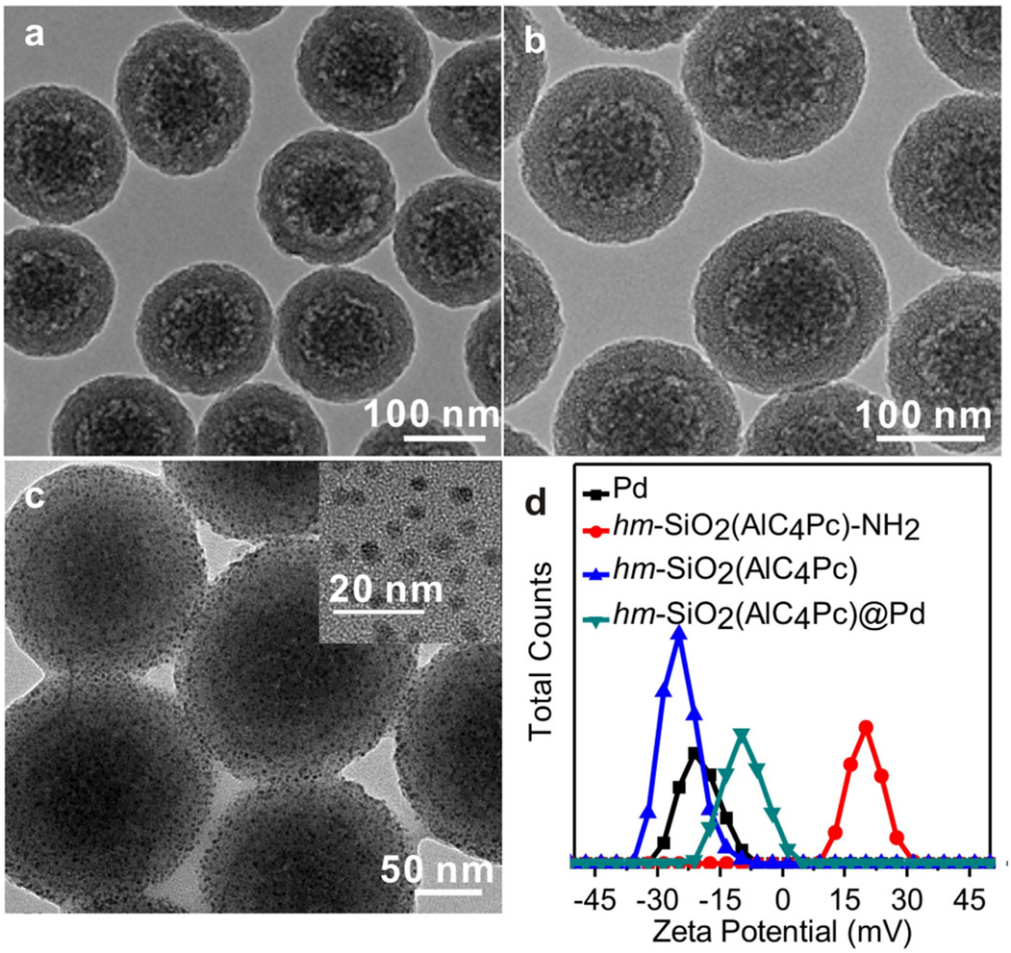

Figure 2. TEM images of the *hm*-SiO_2 (a), *hm*-$SiO_2(AlC_4Pc)$ (b) and *hm*-$SiO_2(AlC_4Pc)$@Pd (c) nanoparticles. Inset in figure 2(c): TEM image of small Pd nanosheets. (d) Zeta potentials of Pd nanosheets, *hm*-$SiO_2(AlC_4Pc)$, *hm*-$SiO_2(AlC_4Pc)$-NH_2 and *hm*-$SiO_2(AlC_4Pc)$@Pd nanoparticles in water.

2.8. Characterization

Transmission electron microscopy (TEM) studies were performed using a TECNAI F-30 high-resolution transmission electron microscope operating at 300 kV. UV/Vis absorption spectra were measured with a Cary 5000 UV/Vis/NIR spectrophotometer (Varian). Zeta-potential experiments were carried out on a Nano-ZS (Malvern Instruments).

3. Results and discussion

3.1. Synthesis and characterization of hm-$SiO_2(AlC_4Pc)$@Pd nanoparticles

The *hm*-$SiO_2(AlC_4Pc)$@Pd nanoparticles were fabricated according to the process depicted in figure 1. In brief, monodisperse solid SiO_2 nanoparticles (*s*SiO_2) were first prepared using a modified Stöber method. The prepared *s*SiO_2 were then coated with CTAB/SiO_2 shell (*s*SiO_2@CTAB/SiO_2) via base-catalyzed hydrolysis of TEOS and condensation of silica onto the surface of CTAB pre-coated *s*SiO_2. Simultaneously, the PS AlC_4Pc were also covalently incorporated into the silica shell by reacting the carboxylic groups of AlC_4Pc with amino groups of APTES in advance to form a AlC_4Pc-APTES conjugate that could co-hydrolyze and condense with TEOS during the *s*SiO_2@CTAB/SiO_2 synthesis step (*s*SiO_2@ CTAB/$SiO_2(AlC_4Pc)$). To evolve *s*SiO_2@CTAB/$SiO_2(AlC_4Pc)$ with hollow cores and penetrating pore channels (*hm*-$SiO_2(AlC_4Pc)$), Na_2CO_3 was utilized to remove *s*SiO_2 core-generating templates and NH_4NO_3 was used to remove CTAB pore-generating templates in turn. Finally, small Pd nanosheets were deposited onto the surface of amino-modified *hm*-$SiO_2(AlC_4Pc)$ nanoparticles to obtain *hm*-$SiO_2(AlC_4Pc)$@Pd nanoparticles.

As shown in the transmission electron microscope (TEM) images of figures 2(a) and (b), after loading AlC_4Pc, the prepared *hm*-$SiO_2(AlC_4Pc)$ nanoparticles had a uniform diameter of ~170 nm (figure 2(b)), which was similar to that of *hm*-SiO_2 (figure 2(a)). The transparency of the core of the *hm*-$SiO_2(AlC_4Pc)$ confirms their hollow characteristics. The shell of the *hm*-$SiO_2(AlC_4Pc)$ with a thickness of ~26 nm displays an obvious wormhole-like mesoporous silica structure generated by the removal of pore templates. The hollow mesoporous silica structure not only improves the hydrophilic property of the PS molecules, but also be helpful to the diffusion of ground state O_2 that interacts with the PSs for

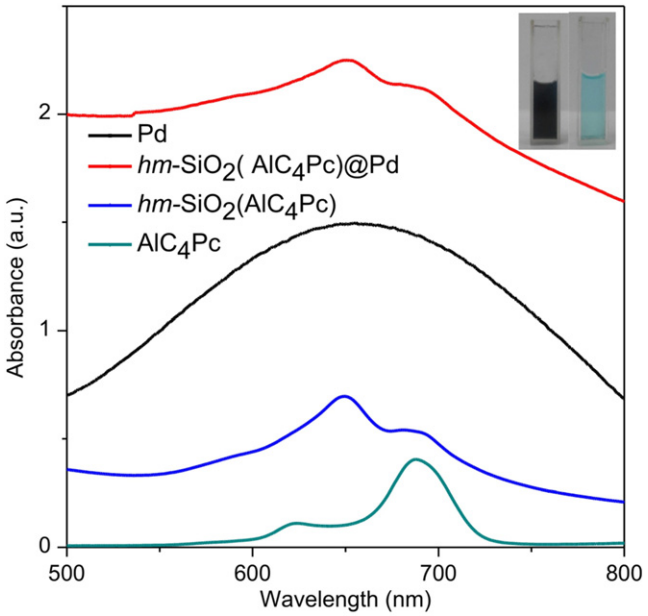

Figure 3. UV-Vis-NIR absorption spectra of free AlC_4Pc, *hm*-$SiO_2(AlC_4Pc)$, Pd nanosheets and *hm*-$SiO_2(AlC_4Pc)$@Pd. Inset, digital photographs of *hm*-$SiO_2(AlC_4Pc)$ (blue) and *hm*-$SiO_2(AlC_4Pc)$@Pd (dark blue) in PBS buffer (pH 7.4).

effective singlet oxygen generation. The generated singlet oxygen can also be easily released from the matrix.

After reacting with APTES, the *hm*-$SiO_2(AlC_4Pc)$ nanoparticles were endowed with amino groups on their surfaces (*hm*-$SiO_2(AlC_4Pc)$-NH_2). These amino-bearing particles have a zeta potential of +21.4 mV (figure 2(d)). Then the negatively charged Pd nanosheets (~4.4 nm in diameter (inset of figure 2(c)) and $\zeta = -21.0$ mV (figure 2(d)) were deposited onto the surface of *hm*-$SiO_2(AlC_4Pc)$-NH_2 by electrostatic and coordination interaction between the amino groups and the Pd nanosheets. As seen from figure 2(c), Pd nanosheets were clearly visible on the surface of *hm*-$SiO_2(AlC_4Pc)$-NH_2, and the zeta potential of *hm*-$SiO_2(AlC_4Pc)$@Pd was −9.6 mV between the values of Pd nanosheets and *hm*-$SiO_2(AlC_4Pc)$-NH_2, implying that the Pd nanosheets were successfully coated on *hm*-$SiO_2(AlC_4Pc)$-NH_2.

3.2. Spectroscopic properties of hm-$SiO_2(AlC_4Pc)$@Pd

Figure 3 shows the UV-Vis-NIR absorption spectra of AlC_4Pc, Pd nanosheets, *hm*-$SiO_2(AlC_4Pc)$ and *hm*-$SiO_2(AlC_4Pc)$@Pd. Free AlC_4Pc has a strong Q-band absorption peak at 687 nm. After conjugating it into silica shell, the characteristic absorption of *hm*-$SiO_2(AlC_4Pc)$ is similar to that of AlC_4Pc, indicating no change in the chromophore upon conjugation. However, an obvious oligomers absorption peak at 650 nm occurs due to the aggregation of AlC_4Pc. The amount of bound AlC_4Pc onto *hm*-$SiO_2(AlC_4Pc)$ was determined indirectly by the difference between the amount of AlC_4Pc-APTES added for the sol-gel reaction and the amount of AlC_4Pc in the supernatant through the calibration curve of AlC_4Pc at 687 nm (figure S1). As shown in figure S2, the amounts of loading AlC_4Pc increased as the rise of adding AlC_4Pc-APTES volume and remained almost invariable at about 1.2 wt% (200 μl AlC_4Pc-APTES). Therefore, *hm*-$SiO_2(AlC_4Pc)$ nanoparticles with 1.2 wt% AlC_4Pc loading was used for our study. After coating Pd nanosheets onto the nanoparticles, *hm*-$SiO_2(AlC_4Pc)$@Pd exhibited an increased absorption band from visible to NIR owing to the wide absorption of Pd nanosheets at the wavelength range of 500–800 nm. Relative to typical milk-white-colored non-AlC_4Pc-containing *hm*-SiO_2 nanoparticle solution (figure S2), a clearly blue-colored water solution (inset of figure 3 and figure S2(b)) could be seen in the sample of *hm*-$SiO_2(AlC_4Pc)$, demonstrating the successful loading of AlC_4Pc within the silica matrix. After anchoring Pd nanosheets onto the nanoparticles, the color of the solution further changed into black-blue (inset of figure 3). Similarly, the loading amount of Pd nanosheets can be calculated to be about 5 wt% according to the calibration curve of Pd nanosheets (figure S3 and figure S4).

Since PS AlC_4Pc were covalently conjugated to the mesoporous silica network of *hm*-$SiO_2(AlC_4Pc)$-NH_2 nanoparticles, and small Pd nanosheets were coated onto their surfaces by electrostatic and coordination interaction, it was expected that the prepared *hm*-$SiO_2(AlC_4Pc)$@Pd displayed good dispersion stability in some physiological solutions, such as phosphate-buffered saline (PBS) and cell culture medium. To test this, both *hm*-$SiO_2(AlC_4Pc)$-NH_2 and *hm*-$SiO_2(AlC_4Pc)$@Pd were dispersed in PBS and RPMI 1640 cell medium with 10% fetal bovine serum (FBS) for 12 h, respectively. After centrifuging, the supernatants were subjected to UV-Vis adsorption measurements. As illustrated in figure S5, no obvious signals of phthalocyanine or Pd nanosheets can be detected from the adsorption spectra of the supernatants in both PBS and RPMI 1640, suggesting that the *hm*-$SiO_2(AlC_4Pc)$-NH_2 and *hm*-$SiO_2(AlC_4Pc)$@Pd nanoparticles were very stable against dye leaching and had excellent dispersion stability in physiological solutions.

3.3. Singlet oxygen generation and photothermal effect of hm-$SiO_2(AlC_4Pc)$@Pd

As a potential second-generation PS, AlC_4Pc has good photodynamic effects because of its intense absorption at the NIR region, which is the penetration window of tissues, and its highly efficient singlet oxygen photogeneration [13]. To verify the production of $^1O_2$ by *hm*-$SiO_2(AlC_4Pc)$@Pd, a chemical method was used by the photodegradation of DPBF, which caused a decrease in DPBF absorption intensity at 411 nm. As shown in figure 4(a), the absorption intensity of DPBF at about 411 nm in *hm*-$SiO_2(AlC_4Pc)$@Pd solutions decreased continuously with the 660 nm laser irradiation (0.1 W cm^{-2}), which is similar to that of *hm*-$SiO_2(AlC_4Pc)$ (line 3 of figure 4(b)). In contrast, no detectable bleaching of the DPBF absorption at 411 nm was observed for the Pd nanosheets under the same irradiation (line 1 of figure 4(b)), confirming that the photo-oxidation of DPBF is a result of a combined effect of *hm*-$SiO_2(AlC_4Pc)$@Pd and light irradiation.

Because small Pd nanosheets conjugated onto the *hm*-$SiO_2(AlC_4Pc)$-NH_2 still maintained their strong absorption in

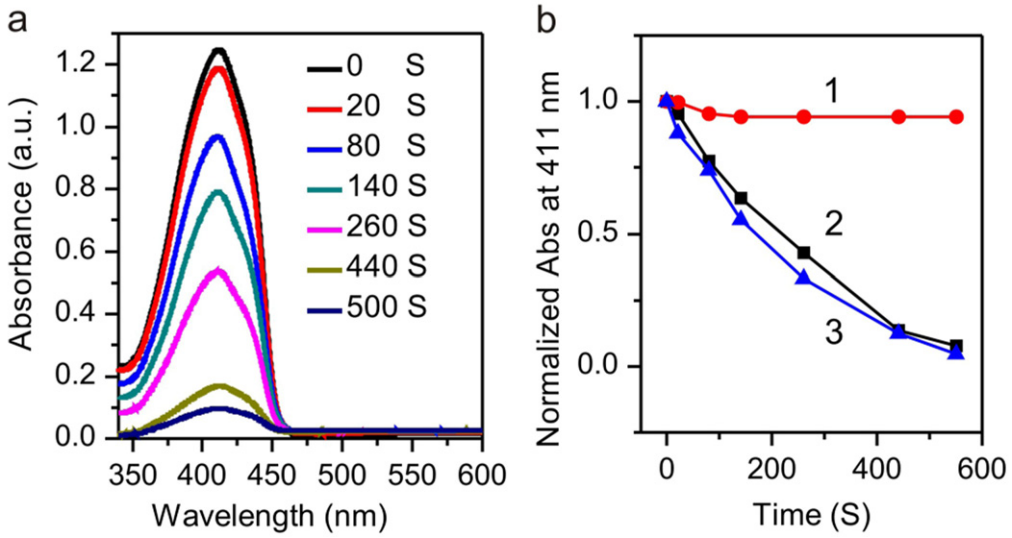

Figure 4. (a) Absorption intensity decreasing of DPBF in *hm*-$SiO_2(AlC_4Pc)$@Pd aqueous solution with the irradiation time of 660 nm light (0.1 W cm^{-2}). (b) Absorption of DPBF at 411 nm as a function of irradiation time in the presence of Pd nanosheets (1), *hm*-$SiO_2(AlC_4Pc)$@Pd (2) and *hm*-$SiO_2(AlC_4Pc)$ (3) aqueous solutions under the irradiation of 660 nm laser (0.1 W cm^{-2}).

the range of 500–800 nm with maximum wavelength located at about 660 nm (figure 3), this inspires us to investigate the photothermal effect of *hm*-$SiO_2(AlC_4Pc)$@Pd under the irradiation of a 660 nm laser (0.5 W cm^{-2}) that is used for the PDT. As illustrated in figure 5, the temperature of 1.0 ml water solution containing 200 μg of *hm*-$SiO_2(AlC_4Pc)$@Pd rapidly increased from 26.4 °C to 37.4 °C after 4 min of 660 nm irradiation. While no significant temperature change was observed for the *hm*-$SiO_2(AlC_4Pc)$ solution under the same irradiation conditions. These data confirm that *hm*-$SiO_2(AlC_4Pc)$@Pd can effectively absorb and convert 660 light energy into heat. Therefore, *hm*-$SiO_2(AlC_4Pc)$@Pd was highly desirable for both cancer cell PDT and PTT.

3.4. Biocompatibility and cell uptake of hm-$SiO_2(AlC_4Pc)$@Pd

Before using the *hm*-$SiO_2(AlC_4Pc)$@Pd for PDT/PTT double therapy, we first evaluated its *in vitro* toxicity to cells. HeLa cells were grown with the cell culture medium containing nanoparticles for 12, 24 and 48 h, respectively, and then cell viability was determined using the MTT assay. Figure 6(a) shows that the nanoparticles at different concentrations have no obvious cytotoxic effect on cell viability after 48 h exposure, even at a high dose up to 400 μg ml^{-1}. When cells incubated with nanoparticles were observed under the microscope, the cells still kept good morphology (figure 6(b)). The results indicate that these nanoparticles have good biocompatibility and would be promising for application in cancer therapy.

To achieve good phototherapeutic effect, the efficient internalization of *hm*-$SiO_2(AlC_4Pc)$@Pd nanoparticles into cells is very important since the cells can easily be destroyed by both heat and $^1O_2$ produced from the nanoparticles. Interesting, as AlC_4Pc are fluorescent molecules, they can also offer a means for cell imaging. To monitor the intracellular uptake of nanoparticles, HeLa cells were incubated with the

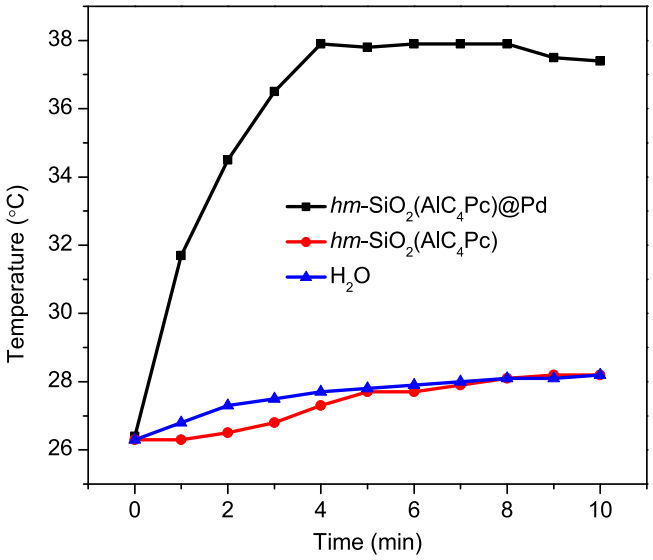

Figure 5. Temperature increase of distilled water, water dispersed *hm*-$SiO_2(AlC_4Pc)$ and *hm*-$SiO_2(AlC_4Pc)$@Pd upon irradiation with a 660 nm laser (0.5 W cm^{-2}). The concentrations of nanoparticles were 200 μg ml^{-1}.

hm-$SiO_2(AlC_4Pc)$@Pd for 4, 8 and 12 h, respectively. After washing the unbound nanoparticles, the cells were imaged by confocal laser microscopy. The cell nuclei were stained with DAPI. It was found that the cellular uptake of *hm*-$SiO_2(AlC_4Pc)$@Pd nanoparticles was time-dependent (figure 7). With the increase of incubation time, more strong red fluorescence emitted by AlC_4Pc from the nanoparticles was observed on the membrane and inside the cytoplasmic regions of the cells (figure 7(d)), implying more nanoparticles were taken in by cells. When the incubation time is 12 h, observation from fluorescent microscopy indicated that there were plenty of nanoparticles in cells. Therefore, 12 h was chosen as the proper incubation time of nanoparticles with cells.

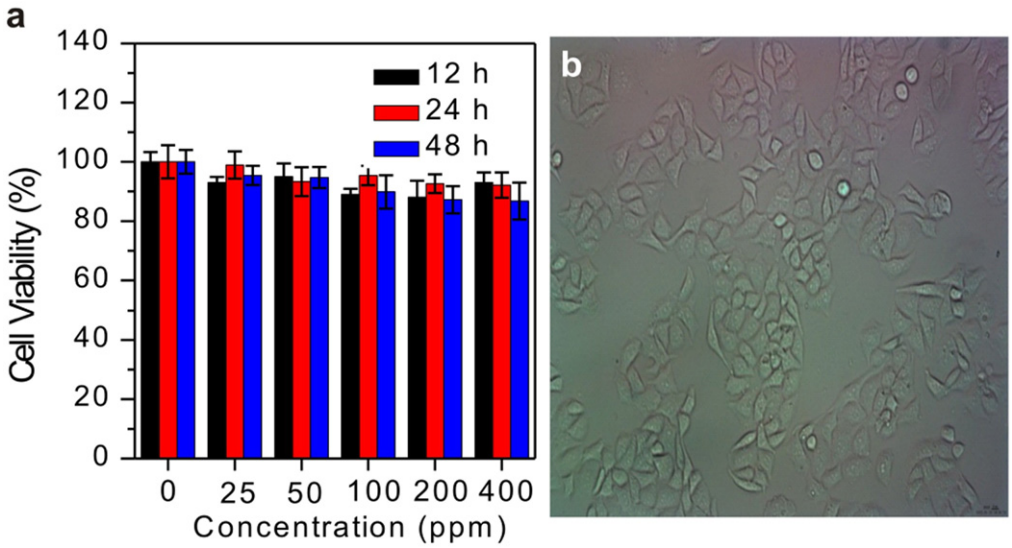

Figure 6. (a) The viability of HeLa cells incubated with different concentrations of *hm*-$SiO_2(AlC_4Pc)$@Pd for 12, 24 and 48 h, respectively. (b) The cell morphology of HeLa cells incubated with *hm*-$SiO_2(AlC_4Pc)$@Pd at 400 μg ml^{-1} for 12 h.

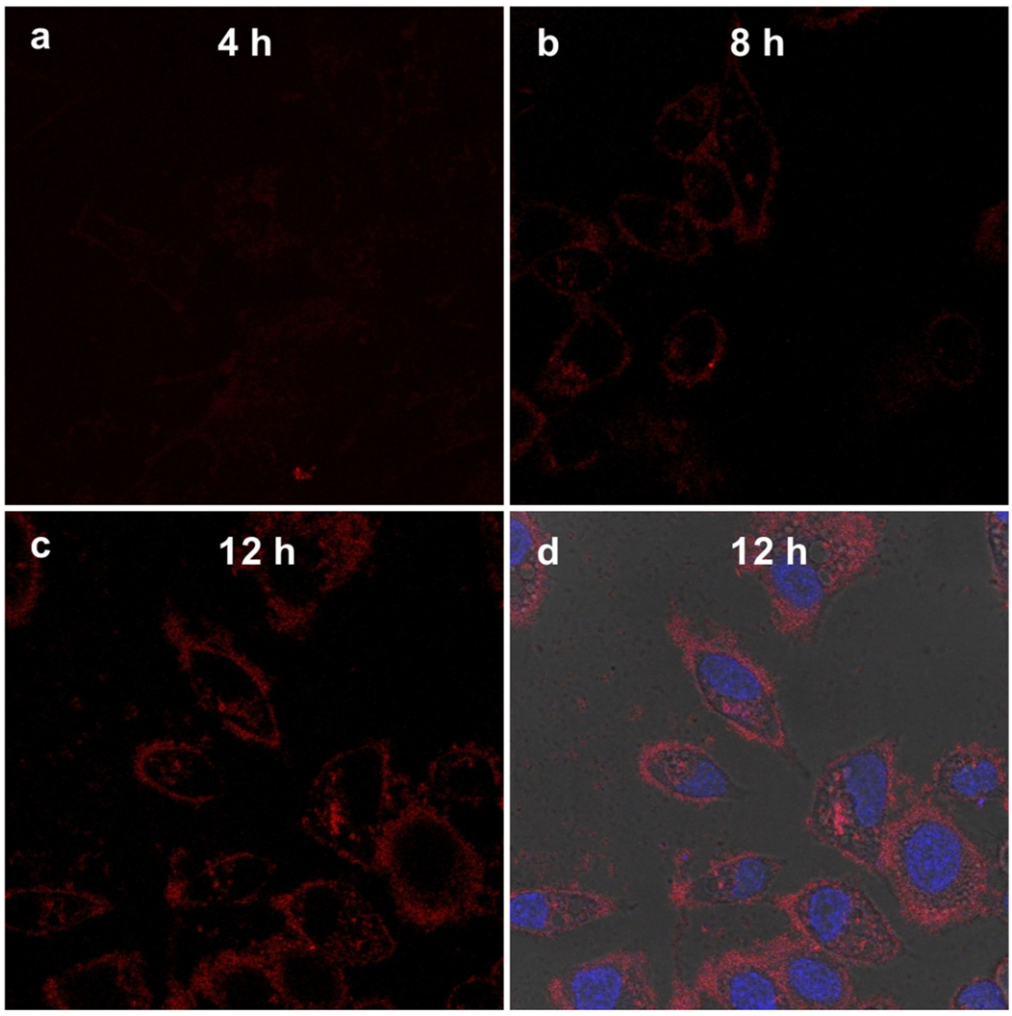

Figure 7. Confocal fluorescence images of HeLa cells after incubation with *hm*-$SiO_2(AlC_4Pc)$@Pd (200 μg ml^{-1}) for 4 (a), 8 (b) and 12 h (c), respectively. (d) Merging of images of nanoparticles, bright-field and DAPI fluorescence after 12 h incubation. The cell nuclei were stained with DAPI (blue fluorescence).

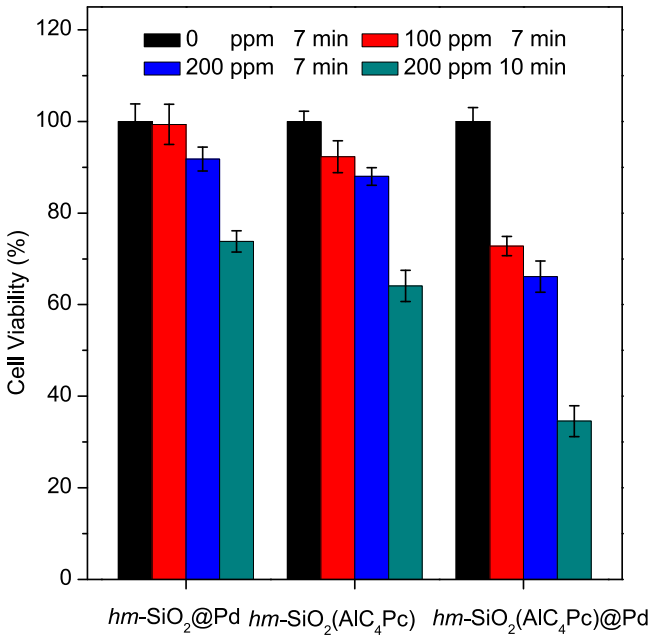

Figure 8. Relative viability of HeLa cells incubated with various concentrations of *hm*-SiO_2@Pd, *hm*-$SiO_2(AlC_4Pc)$ and *hm*-$SiO_2(AlC_4Pc)$@Pd after irradiation by 660 nm laser (0.5 W cm^{-2} for 7 min and 10 min).

3.5. In vitro photodynamic and photothermal double therapy using hm-$SiO_2(AlC_4Pc)$@Pd

To evaluate the feasibility of utilizing the *hm*-$SiO_2(AlC_4Pc)$@Pd for PDT/PTT combined therapy, HeLa cells were incubated with *hm*-SiO_2@Pd (for PTT), *hm*-$SiO_2(AlC_4Pc)$ (for PDT) and *hm*-$SiO_2(AlC_4Pc)$@Pd at the same concentration (100 or 200 μg ml^{-1}) for 12 h and then exposed to the 660 nm laser at a power density of 0.5 W cm^{-2} for 7 or 10 min. A standard MTT assay was carried out to determine the relative viabilities of cells after irradiation. As shown in figure 8, the combined treatment generated a significant cell death at all tested concentrations of *hm*-$SiO_2(AlC_4Pc)$@Pd, compared with *hm*-$SiO_2(AlC_4Pc)$ or *hm*-SiO_2@Pd with the same 660 nm illumination. For example, by using *hm*-$SiO_2(AlC_4Pc)$@Pd for both PDT and PTT, 35% of the cells were killed at the concentration of 200 μg ml^{-1} with laser irradiation for 7 min. In contrast, about 13% or 8% of the cells were killed in the presence of 200 μg ml^{-1} *hm*-$SiO_2(AlC_4Pc)$ or 200 μg ml^{-1} *hm*-SiO_2@Pd, respectively. The cell–killing efficacy by *hm*-$SiO_2(AlC_4Pc)$@Pd was even higher than the sum of PDT by *hm*-$SiO_2(AlC_4Pc)$ and PTT by *hm*-SiO_2@Pd. In addition, it was found that the combined PDT/PTT therapeutic efficacy increased with the extension of irradiation time when the laser power density (0.5 W cm^{-2}) and nanoparticle concentration (200 μg ml^{-1}) were kept invariable. After 10 min of irradiation, cell viability decreased to below 35% for the *hm*-$SiO_2(AlC_4Pc)$@Pd treated cells. Microscopic images of trypan-blue-stained cells (dead cells) after different treatments also confirmed that the phototherapeutic efficiency caused by *hm*-$SiO_2(AlC_4Pc)$@Pd was higher than either *hm*-$SiO_2(AlC_4Pc)$ or *hm*-SiO_2@Pd alone after 10 min of irradiation (figure 9). The results described above indicated that the *hm*-$SiO_2(AlC_4Pc)$@Pd exhibited excellent Pd photothermal therapy and AlC_4Pc photodynamic therapy with a synergistic effect.

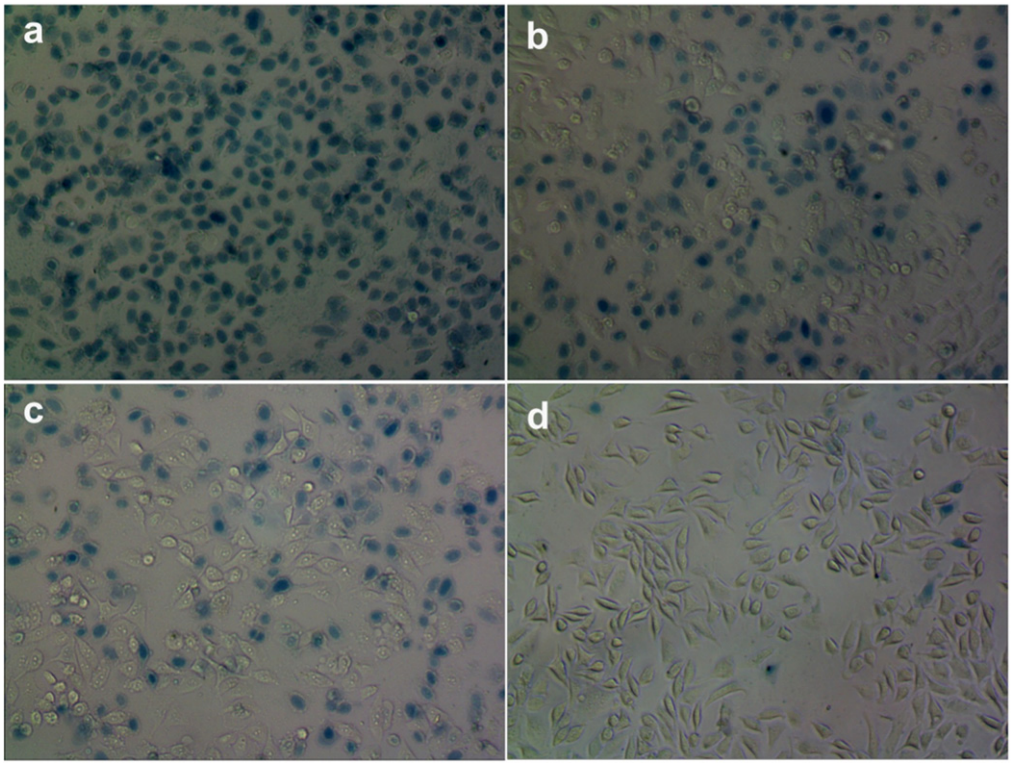

Figure 9. Optical image of trypan-blue-stained HeLa cells incubated with 200 μg ml^{-1} *hm*-$SiO_2(AlC_4Pc)$@Pd (a), *hm*-$SiO_2(AlC_4Pc)$ (b), *hm*-SiO_2@Pd (c) and without nanoparticles (d) after 660 nm laser irradiation (0.5 W cm^{-2} for 10 min).

4. Conclusion

In summary, *hm*-SiO_2(AlC_4Pc)@Pd have been successfully designed for PDT/PTT double phototherapy using a single laser (660 nm). In the nanocomposite, highly uniform, monodisperse, and hollow mesoporous silica nanoparticles that comprise PSs AlC_4Pc for PDT and Pd nanosheets for PTT. The prepared *hm*-SiO_2(AlC_4Pc)@Pd exhibited good biocompatibility, easy uptake by cancer cells, high efficiency in photogenerating cytotoxic singlet oxygen and excellent photothermal conversion capacity, which can guarantee good therapeutic efficacy. *In vitro* cancer therapy of the multifunctional nanoparticles was evaluated. The results demonstrated that a cooperative therapeutic system combining PDT and PTT can produce remarkable therapeutic efficacy relative to individual means.

Acknowledgements

We thank Professor Nanfeng Zheng for helpful discussions and comments on the manuscript. The work was supported by the National Natural Science Foundation of China (No.21101131), the National Basic Research Foundation (973) of China (2014CB932004), the Natural Science Foundation of Fujian Province (No.2012J01056), the Fundamental Research Funds for the Central Universities (2010121015), the open project grant from State Key Laboratory of Chemo/Biosensing and Chemometrics (2013009), and the Scientific Research Foundation for the Returned Overseas Chinese Scholars of State Education Ministry.

References

[1] Triesscheijn M, Baas P, Schellens J H and Stewart F A 2006 Photodynamic therapy in oncology *Oncologist* **11** 1034–44
[2] Moore C M, Pendse D and Emberton M 2009 Photodynamic therapy for prostate cancer—a review of current status and future promise *Nat. Clin. Practice Urology Rev.* **6** 18–30
[3] Detty M R, Gibson S L and Wagner S I 2004 Current clinical and preclinical photosensitizers for use in photodynamic therapy *J. Med. Chem.* **47** 3897–915
[4] Chatterjee D K, Li S F and Zhang Y 2008 Nanoparticles in photodynamic therapy: an emerging paradigm *Adv. Drug Deliv. Rev.* **60** 1627–37
[5] Konan Y, Gurny R and Allemann E 2002 State of the art in the delivery of photosensitizers for photodynamic therapy *J. Photochem. Photobiol.* B **66** 89–106
[6] Bechet D, Couleaud P, Frochot C, Viriot M L, Guillemin F and Barberi-Heyob M 2008 Nanoparticles as vehicles for delivery of photodynamic therapy agents *Trends Biotechnol.* **26** 612–21
[7] Juzenas P, Chen W, Sun Y P, Coelho M A N, Generalov R, Generalova N and Lie I C 2008 Quantum dots and nanoparticles for photodynamic and radiation therapies of cancer *Adv. Drug Delivery Rev.* **60** 1600–14
[8] Chen W and Zhang J 2006 Using nanoparticles to enable simultaneous radiation and photodynamic therapies for cancer treatment *J. Nanosci. Nanotechnol.* **6** 1159–66
[9] Cheng S H, Lee C H, Yang C S, Tseng F G, Mou C Y and Lo L W 2009 Mesoporous silica nanoparticles functionalized with an oxygen-sensing probe for cell photodynamic therapy: potential cancer theranostics *J. Mater. Chem.* **19** 1252–7
[10] Zhang R R, Wu C L, Tong L L, Tang B and Xu Q H 2009 Multifunctional core-shell nanoparticles as highly efficient imaging and photosensitizing agents *Langmuir* **25** 10153–8
[11] Qian H S, Guo H C, Ho P C L, Mahendran R and Zhang Y 2009 Mesoporous-silica-coated up-conversion fluorescent nanoparticles for photodynamic therapy *Small* **5** 2285–90
[12] Zhu J, Wang H X, Liao L, Zhao L Z, Zhou L, Yu M H, Wang Y H, Liu B H and Yu C Z 2011 Small mesoporous silica nanoparticles as carriers for enhanced photodynamic therapy *Chem. Asian J.* **6** 2332–8
[13] Wang F, Chen X L, Zhao Z X, Tang S H, Huang X Q, Lin C H, Cai C B and Zheng N F 2011 Synthesis of magnetic, fluorescent and mesoporous core-shell-structured nanoparticles for imaging, targeting and photodynamic therapy *J. Mater. Chem.* **21** 11244–52
[14] Wang T T, Zhang L Y, Su Z M, Wang C G, Liao Y and Fu Q 2011 Multifunctional hollow mesoporous silica nanocages for cancer cell detection and the combined chemotherapy and photodynamic therapy *ACS Appl. Mater. Interfaces* **3** 2479–86
[15] Shi S G, Zhu X L, Zhao Z X, Fang W J, Chen M, Huang Y Z and Chen X L 2013 Photothermally enhanced photodynamic therapy based on mesoporous Pd@Ag@mSiO2 nanocarriers *J. Mater. Chem.* B **1** 1133–41
[16] Peng J J, Zhao L Z, Zhu X J, Sun Y, Feng W, Gao Y H, Wang L Y and Li F Y 2013 Hollow silica nanoparticles loaded with hydrophobic phthalocyanine for near-infrared photodynamic and photothermal combination therapy *Biomaterials* **34** 7905–12
[17] Zhang M F, Murakami T, Ajima K, Tsuchida K, Sandanayaka A S D, Ito O, Lijima S and Yudasaka M 2008 Fabrication of ZnPc/protein nanohorns for double photodynamic and hyperthermic cancer phototherapy *Proc. Natl. Acad. Sci. USA* **105** 14773–8
[18] Jang B, Park J Y, Tung C H, Kim I H and Choi Y 2011 Gold nanorod-photosensitizer complex for near-infrared fluorescence imaging and photodynamic/photothermal therapy *in vivo ACS Nano* **5** 1086–94
[19] Tian B, Wang C, Zhang S, Fang L Z and Liu Z 2011 Photothermally enhanced photodynamic therapy delivered by nano-graphene oxide *ACS Nano* **5** 7000–9
[20] Khlebtsov B *et al* 2011 Nanocomposites containing silica-coated gold_silver nanocages and Yb-2,4-dimethoxyhematoporphyrin: multifunctional capability of IR-luminescence detection, photosensitization, and photothermolysis *ACS Nano* **5** 7077–89
[21] Wang J *et al* 2012 Assembly of aptamer switch probes and photosensitizer on gold nanorods for targeted photothermal and photodynamic cancer therapy *ACS Nano* **6** 5070–7
[22] Tang S H, Chen M and Zheng N F 2014 Sub-10 nm Pd nanosheets with renal clearance for efficient near-infrared photothermal cancer therapy *Small* at press
[23] Huang X Q, Tang S H, Mu X L, Dai Y, Chen G X, Zhou Z Y, Ruan F X, Yang Z L and Zheng N F 2011 Freestanding palladium nanosheets with plasmonic and catalytic properties *Nat. Nanotechnol.* **6** 28–32
[24] Huang X Q, Tang S H, Liu B J, Ren B and Zheng N F 2011 Enhancing the photothermal stability of plasmonic metal nanoplates by a core-shell architecture *Adv. Mater.* **23** 3420–5
[25] Chen F P and Xu D Y 1990 Synthesis of water soluble phthalocyanines *Youji Huaxue* **10** 550–3